Optical properties of quantum-wire arrays in (Al,Ga)As serpentine-superlattice structures

H. Weman
Department of Physics and Measurement Technology, Linköping University, S-581 83, Linköping, Sweden

M. S. Miller
Department of Electrical and Computer Engineering, University of California, Santa Barbara, California 93106

C. E. Pryor
Department of Physics, University of California, Santa Barbara, California 93106

Y. J. Li
Department of Electrical and Computer Engineering, University of California, Santa Barbara, California 93106

P. Bergman
Department of Physics and Measurement Technology, Linköping University, S-581 83, Linköping, Sweden

P. M. Petroff and J. L. Merz
Department of Electrical and Computer Engineering, University of California, Santa Barbara, California 93106
(Received 29 December 1992)

Serpentine superlattices with a built-in quantum-wire array have been grown on vicinal (100) GaAs substrates by molecular-beam epitaxy. The quantum wires have parabolic cross sections with confinement dimensions on the order of 100 Å. The goal of this paper is to make a comprehensive optical study of two different serpentine-superlattice samples. The serpentine structures have been characterized by low-temperature cathodoluminescence, photoluminescence, and photoluminescence-excitation measurements. In photoluminescence, a rather sharp peak (typically 7 meV full width at half maximum) is attributed to excitonic recombination in the built-in quantum-wire array. The linear polarization dependence of the serpentine-superlattice emission has been measured with a photoelastic modulation technique, showing a pronounced polarization anisotropy in both photoluminescence and photoluminescence excitation. The serpentine-superlattice photoluminescence emission normal to the vicinal surface shows a linear polarization along the wires of up to about 30% due to the lateral confinement. The carrier confinement has been further characterized by measuring the linear polarization dependence of the photoluminescence normal to the cleaved edges. The measured polarization anisotropy has been compared with the calculated polarization dependence as a function of intermixing between the lateral barriers and wells. It is found that there is a substantial intermixing between the barriers and wells, with at least 30% of the Al intended for the barrier ending up in the well. This results in hole states confined to one dimension, while the electron states are two dimensional due to coupling through the lateral barriers. Linearly polarized photoluminescence excitation has been used to reveal the laterally induced heavy-hole–light-hole splitting. Photoluminescence decay-time measurements of the serpentine-superlattice emission (390 ps) show a longer radiative decay time at low temperature than for a reference alloy-well structure (260 ps), indicating a reduced recombination rate in the serpentine structure. The linear polarization of the photoluminescence is found to be rather constant over large areas of the wafer even though the growth rate varies by a few percent. This indicates that uniform quantum-wire-like states are formed and demonstrates the intended advantage of the serpentine superlattice, which avoids the tilt sensitivity of the tilted superlattice.

I. INTRODUCTION

Recently there has been a considerable interest in low-dimensional quantum structures where the carrier motion is confined to one (quantum wire) or zero (quantum box) dimensions. These structures are expected to have dramatically improved optical and transport properties with a large potential for future device applications.[1] Different approaches have been taken to fabricate quantum structures: by electron-beam lithography,[2,3] focused ion-beam technology,[4] or by direct growth on either vicinal[5] or patterned substrates.[6]

Etched quantum structures have very recently been made where it is possible to spectrally resolve higher quantum-wire subbands.[3,7,8] The optical properties of these quantum wires are also expected to show enhanced oscillator strengths, nonlinear effects, and increased excitonic binding energies compared to the quantum-well case due to the peaked nature of the one-dimensional (1D) density of states.[9] An enhanced binding energy and

0163-1829/93/48(11)/8047(14)/$06.00

an enhanced reduced mass has been reported for excitons in etched quantum wires.[2] However, there is no experimental evidence for an enhanced oscillator strength; rather there are several indications of a reduced optical efficiency and a reduced carrier relaxation in different 1D systems.[7,10] Another effect of the laterally induced confinement is that it causes an optical anisotropy in the plane of the original well. The optical selection rules for 1D systems have been treated theoretically[11–13] and experimentally from photoluminscence (PL) and photoluminescence excitation (PLE) studies of various types of quantum wires[14–16] and are often used as a proof for the quantum-wire confinement. However, when the lateral potential is induced by strain,[14] the observed optical anisotropy can also be explained by the anisotropy of the strain field.[17,18]

The growth of AlAs/GaAs "tilted superlattices" (TSL's) on vicinal substrates has provided a promising way to fabricate quantum-well-wire arrays with a lateral width of just a few nanometers.[5,19] Cross-section transmission electron microscopy (TEM) micrographs of these structures do show evidence of a lateral composition modulation.[5] A large optical anisotropy in polarized photoluminescence excitation was reported for a GaAs quantum well (QW) corrugated with a TSL barrier.[20] Recent calculations by Citrin and Chang,[11] however, showed that much smaller anisotropy is expected, even for an ideally corrugated QW without any lateral intermixing, and it has since been shown that the claimed polarization anisotropy observed in Ref. 20 arose from experimental artifacts.[21] Similar anisotropy was also reported for a single monolayer lateral superlattice inserted in the center of a QW,[22] which is consistent with the prediction that even elongated AlAs islands in GaAs QW's should cause an optical anisotropy.[23]

One of the major problems when growing an AlAs/GaAs TSL on a vicinal (100) GaAs substrate is the thermodynamic and kinetic difficulty of having the Al incorporate only at the step edge and not out on the terrace. This results in incomplete segregation into the lateral wells and barriers and a final structure that is not too different from the average alloy composition. Thus when the overall average Al composition of the lateral superlattice is larger than about 40%, this can result in an indirect band-gap structure. This can be solved by using digital-alloy barriers, where the barrier is made of an alternate sequence of GaAs and AlAs partial layers in the vertical direction, as shown in Fig. 1(a). By, e.g., lowering the intended Al concentration in the barrier to 50%, the resulting average Al composition in the lateral superlattice is 25% for barriers nominally intended to cover $\frac{1}{2}$ a step, which will result in a direct band-gap structure even with incomplete segregation. With the digital-alloy barrier, this reduction may be accomplished without reducing the width of an already thin barrier. Another problem intrinsic to the TSL growth geometry is that the tilt angle is not a well-controlled parameter. The electronic confinement energies will change with the tilt angle, and as a result the optical and electrical properties are not well controlled in a TSL. Recently we have presented a way to avoid this problem by purposely changing the tilt angle so that a crescent-shaped well is achieved.[24,25] The resulting structure, which we have named a serpentine superlattice (SSL), inherently accommodates the geometric sensitivity to absolute growth rates.

A schematic diagram of a parabolic SSL that would result from a linear sweep of the deposition is shown in Fig. 1(b). The x, y, and z axes are defined as parallel to the wires, in the periodic direction, and normal to the array, respectively. The step height is d and the substrate misorientation angle is α, giving terraces of width $W=d/\sin\alpha$. The linear sweep of the deposition is characterized by the change in coverage Δp with thickness grown Δz. A ramping constant is defined here by the parameter z_0, where $1/z_0=\Delta p/\Delta z$. The parabolic arcs that describe the lateral barrier and well interfaces are given by $y=z^2/2r$, where the radius of curvature at the vertices is $r=z_0\tan\alpha$. The electronic states are confined near the vertices of the parabolas, where the height of the wire is given by the span of the arc at a point halfway between the lateral barriers, as indicated in

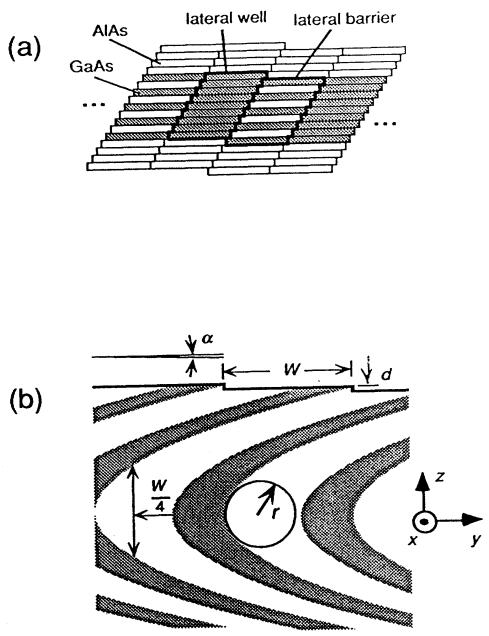

FIG. 1. (a) Lateral superlattice with digital alloy barriers. The GaAs is indicated by the shaded and AlAs by the white partial layers. The Al content in the lateral AlGaAs barrier is $x_{\text{barrier}}=\frac{1}{2}$. (b) Schematic figure of a serpentine superlattice (SSL) with a parabolic cross section produced by an alternate fractional monolayers of AlAs and GaAs. The step height is d and the substrate misorientation angle is α, giving terraces of width $W=d/\sin\alpha$. The parabolic arcs that describe the lateral barrier and well interfaces are given by $y=z^2/2r$, where r is the radius of curvature at the vertices. The electronic states are confined near the vertices of the parabolas, where the height of the wire is given by the span of the arc at a point halfway between the lateral barriers. The definition of the x, y, and z axes for the serpentine-superlattice sample used throughout the paper is also shown.

Fig. 1(b). In contrast to the lateral superlattices reported in Refs. 15, 20, and 22, which will *perturb* the QW's, ideal SSL structures are expected to *confine* states to 1D. From the polarization anisotropy[25] and diamagnetic shift anisotropy,[26] 1D confinement effects have been demonstrated recently for the SSL structure.

The purpose of this paper is to make a comprehensive luminescence study of two different SSL samples. The outline of the paper is as follows: In the experimental part (Sec. II) we describe the growth of the SSL samples (II A) as well as the experimental techniques used (II B). The experimental techniques are based on luminescence spectroscopy using PL and cathodoluminescence (CL). In Sec. III we describe the experimental results showing PL and CL spectra (III A), linearly polarized PL spectra (III B), and linearly polarized PLE spectra (III C). The intensity, lifetime, and uniformity dependence of the PL emission are shown in Sec. III D. In Sec. IV we discuss the interpretation of the results, showing that the PL peak is excitonic and originates from the intended serpentine-superlattice structure (IV A). The amount of lateral confinement is estimated from the linearly polarized PL data in terms of the intermixing between the barrier and wire in the SSL structure (IV B). Other effects that are interpreted to be due to the lateral confinement are discussed in Sec. IV C. This includes the linearly polarized PLE anisotropy and a longer radiative decay time in the SSL structure compared to a reference alloy well. Growth-rate variations and its influence on the uniformity of the formed quantum wires are discussed in Sec. IV D. Finally, in Sec. V we summarize our conclusions from this study and make some suggestions for future studies.

II. EXPERIMENT

A. Sample preparation

We have studied a number of different SSL structures grown on vicinal (100) GaAs substrates. The substrates were misoriented towards the (111) plane, giving Ga-terminated or "*A*"-type step edges. The vicinal misorientation angles α investigated were 0.5°, 1.0°, 1.5°, and 2.0°, corresponding to stepped surfaces with lateral periods of 324, 162, 108, and 81 Å, respectively. The parabolic curvatures are determined by the misorientation angle and $1/z_0$, the linear ramping of the per-cycle coverage per layer thickness. Values of z_0 studied have ranged from 125 to 509 nm. The digital alloy barriers have had nominal AlAs contents ranging from $\frac{1}{5}$ to 1. The intended structures have been observed in TEM diffraction patterns and images,[25,27] though the AlAs is seen to be unintentionally present in the lateral wells in addition to the barriers. The SSL layers are clad above and below with thick $Al_xGa_{1-x}As$ layers to confine the photoexcited carriers to the SSL region. These cladding layers in turn contain quantum wells that serve as optical references.

The structure were grown in a Varian Gen. II molecular-beam epitaxy (MBE) machine, with the molecular-beam shutters under computer control and having a shuttering resolution of 20 ms. The SSL's are grown with an alternating molecular-beam epitaxy (AMBE) technique, alternating between column-III and As_4 molecular beams.[28] Most other layers in the samples were grown with the conventional simultaneous molecular-beam epitaxy (SIMBE) technique. Nominal column-III fluxes were set to continuous growth rates of 0.25–0.5 monolayers/s, giving effective growth rates of 0.05–0.15 monolayers/s during AMBE. The As_4 to column-III flux ratios were 10:1 to 15:1, and the As_4 on to off ratio was typically 12:1. The substrate temperatures were around 600° to 610 °C during SSL growth. The substrates were smoothed by first growing a few thousand angstroms of GaAs at 620 °C and then a 20-period 25-Å AlAs–15-Å GaAs smoothing superlattice.

Two SSL samples and an alloy-well model sample are reported upon in detail in this paper. They are representative of the samples we have studied. The details of the structures and compositions for these samples are given in Table I. Sample 1 contains four successive arrays of parabolic crescents, forming two successive S shapes, and was grown on a 2°-misoriented substrate. TEM micrographs[27] indicate that the nominal Ga flux was approximately 5% higher than assumed during growth, shifting the arcs upwards and downwards, though maintaining the intended parabolic cross sections. The ramping constant was 509 nm, with a total SSL layer thickness of 4080 Å. The lateral barriers were nominally intended to cover $\frac{3}{7}$ of a step and have a digital alloy composition of $x_{\text{barrier}}=\frac{1}{2}$. The sample was grown without rotating the substrate. The lower cladding layer is $Al_{0.3}Ga_{0.7}As$ and contains one 100-Å quantum well while the upper cladding was $Al_{0.35}Ga_{0.65}As$ and contains four 15-Å quantum wells.

The other SSL structure, sample 2*b*, contains a single array of parabolic crescents grown on a 2° misoriented substrate. The ramping constant was 174 nm, with a total SSL layer thickness of 510 Å. The lateral barriers were nominally intended to cover $\frac{1}{2}$ of a step and have a digital alloy composition of $x_{\text{barrier}}=\frac{1}{3}$. The sample was

TABLE I. Sample parameters for the serpentine-superlattice structures used in this paper, grown on vicinal (100)GaAs substrates tilted towards the (111) plane. α is the substrate misorientation angle, z the growth direction coordinate, and $1/z_0$ the per-monolayer ramping rate of the coverage.

Sample no.	Substrate misorientation (α)	Number of crescents	Barrier/terrace width (m)	Al composition in barrier (x_{barrier})	Ramping constant (z_0) (nm)	Reference QW width (Å)
1	2°	4	$\frac{3}{7}$	$\frac{1}{2}$	509	100+15(×4)
2*b*	2°	1	$\frac{1}{2}$	$\frac{1}{3}$	174	60+80

grown while synchronously rotating the substrate at a rate corresponding to a full rotation during a given Ga or Al partial-monolayer deposition. The lower cladding layer is $Al_{0.3}Ga_{0.7}As$ and contains one 60-Å and one 80-Å quantum well. The companion sample to 2*b* is sample 2*a*, which incorporates the same buffering and cladding layers and quantum wells, but replaces the SSL with an alloy-well model structure of the same thickness and average composition. This model was prepared on a nominally flat (100) substrate with the model layers grown at 540 °C by SIMBE to suppress lateral segregation of Al and Ga, providing a uniform alloy structure.

B. Experimental setup

For the PL experiments we used the 2.411-eV (5140-Å) line from an Ar^+ ion laser (Coherent Innova 200). The PLE experiments were performed with a tunable Ti:sapphire laser (Spectra Physics Model 3900). The laser beam from the Ar^+ ion laser is vertically polarized whereas the laser beam from the Ti:sapphire is horizontally polarized. The laser beam was focused on the sample using either a cylindrical or spherical lens with the power adjusted typically to give an optical power density of 1 W/cm^2, unless otherwise stated. The emitted light was dispersed through a Spex-1404 0.85-m double grating spectrometer and detected with a cooled GaAs photomultiplier using conventional lock-in techniques. The samples were mounted in a variable-temperature liquid-helium cryostat (Oxford MD3) and usually pumped to a temperature of 1.4 K. The cryostat windows were made of fused quartz (Spectrosil WF) and were found to be totally isotropic down to liquid-helium temperature.

Time-decay measurements were performed with a mode-locked Ar^+ ion laser synchronously pumping a cavity dumped dye laser (Rhodamin 6G or Pyridine 2) resulting in a final pulse width of 5 ps. The luminescence was detected with a microchannel-plate photomultiplier-tube with *S*1 response, and the decays were obtained using a time-correlated photon-counting technique. The time resolution of the system is better than 100 ps.

The CL measurements were performed at 15 K in a modified high-resolution scanning transmission electron microscope (JEOL JSEM 1200 EXII) operated at 120 keV.

For the polarized PL and PLE experiments we have used a photoelastic modulator (PEM) (Hinds model FS-5) whereby the linear polarization of the light is directly modulated and detected.[29] The experimental setup, sketched in Fig. 2(a) for PL and Fig. 2(b) for PLE, consists of the PEM followed by a Glan-Thompson polarizer with the optical axes oriented by 45° to each other. To detect the linear polarization component of the light, the 2*f* signal at 100 kHz (twice the modulation frequency) of the PEM is detected. Since the output intensity after the PEM depends linearly on the input intensity, a normalization of the polarization spectrum has to be performed.[29] This is done by dividing the collected polarization spectrum digitally by the measured PL signal taken with the PEM tuned to the first zero of the zeroth-order Bessel function. The polarization of the light traveling in the *z* direction is defined as

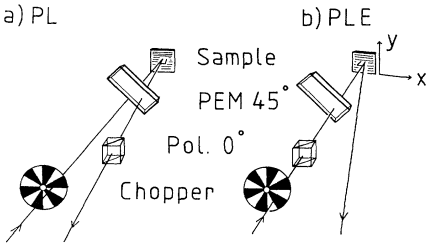

FIG. 2. The experimental setup used to measure the linear polarization of the (a) photoluminescence and (b) photoluminescence excitation. The setup involves a photoelastic modulator (PEM) for direct modulation of the polarization of the emitted luminescence or exciting laser light (Ref. 29).

$$P_z=(I_x-I_y)/(I_x+I_y) \tag{1}$$

where I_x and I_y are the intensity of the emission in the *x* and *y* directions, respectively. [The polarization of the light traveling in the *x* and *y* direction, P_x and P_y, is defined by a cyclic permutation of the indices of Eq. (1).] When using the PEM technique the linear polarization is obtained by measuring the PL intensity (I_{PL}) with the PEM switched off and on, while tuned to the first maximum of the second-order Bessel function. The linear polarization in the *z* direction, P_z, is then determined by

$$P_z=\frac{\{I_{PL}(\text{PEM off})/I_{PL}(\text{PEM on})\}-1}{1+0.28\times\{I_{PL}(\text{PEM off})/I_{PL}(\text{PEM on})\}} . \tag{2}$$

In the polarized PL experiments the exciting light was about 15° off normal incidence and the backscattered luminescence light was detected normal to the surface. When the polarized PL emission was collected from the cleaved facets it was important to excite the sample onto the cleaved facet and not on the vicinal (100) surface to avoid self-absorption of the edge emitting PL and to avoid any mixing of the more intense PL emission from the surface. Therefore we used the same geometry for the polarized PL experiments on the cleaved facets as from the surface. In the polarized PLE experiments the exciting light was at normal incidence and the backscattered luminescence light was detected at about 15° off normal incidence.

III. EXPERIMENTAL RESULTS

A. Photoluminescence

A PL spectrum taken at 1.4 K of sample 1 (a layer of four arrays of serpentine crescents) grown on a 2°-misoriented substrate is shown in Fig. 3. A rather sharp PL peak at 1.823 eV (labeled *A*) with a full width at half maximum (FWHM) of about 14 meV is observed with two shoulder peaks at 1.804 eV [*B*(1)] and 1.792 eV [*B*(2)]. A very broad PL emission (*C* band) is also seen at lower energies. The peak at 1.880 eV is attributed to the four 15-Å QW's (22-meV FWHM) in the upper cladding and the peak at 1.556 eV to the 100-Å QW (4-meV FWHM) in the lower cladding, and will be used as references in the polarization measurements. The *A* peak

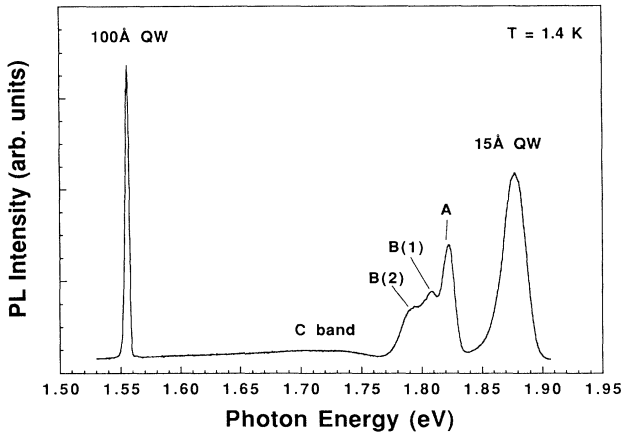

FIG. 3. Photoluminescence spectrum at 1.4 K of sample 1, which contains four vertically displaced arrays of serpentine superlattices (2*S*) grown on a 2° misoriented substrate. The *A*, *B*(1), and *B*(2) peaks and the *C* band are attributed to the serpentine superlattice. The PL peaks from the 100-Å QW and four 15-Å QW's are used for reference measurements. The pump energy was 2.411 eV (5140 Å) and the pump intensity was close to 1 W/cm^2.

originates from the SSL structure, as has been verified by making a spatially resolved CL linescan on the cleaved edge of the sample, as shown in Fig. 4. It can clearly be seen that the *A* peak emission (dotted line) originates from the SSL region between the emission from the 100-Å QW (solid line) in the lower cladding and the four 15-Å QW's (dashed line) in the upper cladding. The *B*(1) and *B*(2) peaks and the *C* band are also attributed to the serpentine-superlattice structure as was verified from PLE, where it was found that these low-energy features are resonantly excited via the *A* peak.

The PL spectra at 1.4 K of sample 2*a*, grown on a nominally flat substrate (dashed line), and sample 2*b*, grown on a 2°-misoriented substrate (solid line), are shown in Fig. 5. The SSL region on the flat substrate is intended to grow without any lateral segregation and should therefore correspond to an $Al_xGa_{1-x}As$ alloy with nominal composition $x = 16.7\%(\frac{1}{2}\times\frac{1}{3})$. Each spectrum consists of three emission lines, where the peaks at 1.565 eV (FWHM of 4 meV for the 0° SSL model and 5.5 meV for the 2° SSL) and 1.593 eV (FWHM of 6 meV for the 0° SSL and 7 meV for the 2° SSL) are due to the 80-Å and 60-Å reference QW's. The peaks at higher energies are attributed to the SSL regions, with the peak at 1.735 eV (7.5-meV FWHM) due to the emission from the SSL quantum wire array and the peak at 1.747 eV (4-meV FWHM) from the alloy-well model. The 2° SSL peak has twice the linewidth of the alloy-well model and shows only a very weak emission tail at lower energies. The spectra in Fig. 5 were chosen from among several that were taken at different positions in order to have the QW peaks lining up at about the same energy. This ensures that the well widths and alloy compositions were fairly similar at these positions on both substrates.

B. Linearly polarized photoluminescence

To further investigate if the SSL peaks in samples 1 and 2*b* show any one-dimensional properties we have performed detailed polarization measurements. The spectra in Fig. 6 have been measured on sample 1, while observing the light emitted in the *z* direction, and using a Glan-Thompson prism to analyze the light parallel (along the *x* direction) and perpendicular (along the *y* direction) to the wires. A clear polarization anisotropy is seen for the *A* peak and the *C* band with a stronger emission along the

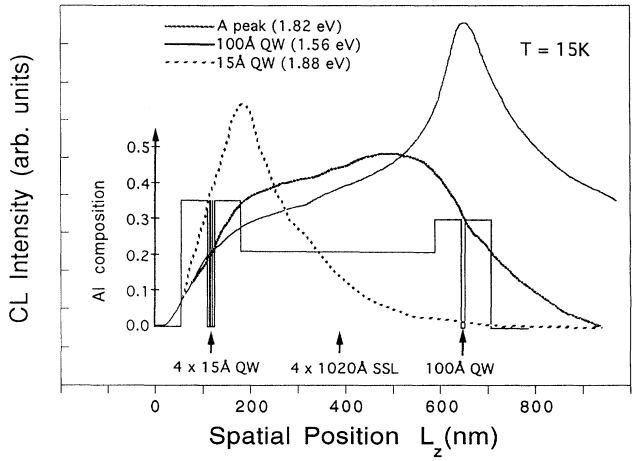

FIG. 4. Spatial cathodoluminescence (CL) line scan onto the cleaved facet of sample 1 taken at 15 K. The spatially dependent CL intensity in the *z* direction (L_z) is shown overlaying a diagram of the intended Al distribution in the structure. The *A* peak (dotted line) luminescence is seen to originate in the SSL region between the 100-Å QW (solid line) in the lower cladding and the four 15-Å QW's (dashed line) in the upper cladding.

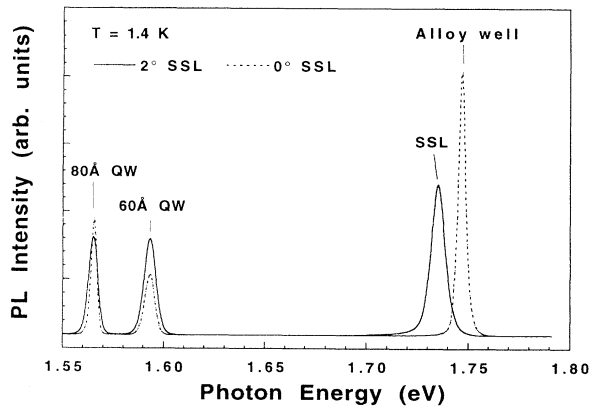

FIG. 5. Photoluminescence spectrum at 1.4 K of sample 2*a* grown on a nominally flat (dashed line) and sample 2*b* grown on a 2° misoriented substrate (solid line). The peak at 1.735 eV is due to the 2° serpentine superlattice and the peak at 1.747 eV is due to the alloy well (0° SSL). The peaks at 1.565 and 1.593 eV are due to an 80-Å and a 60-Å reference QW. The pump energy was 2.411 eV (5140 Å) and the pump intensity was close to 1 W/cm^2.

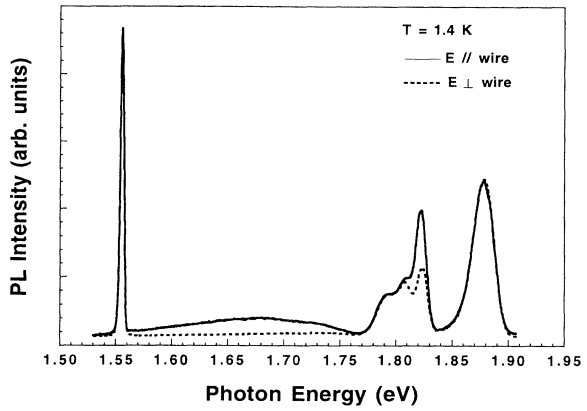

FIG. 6. Polarization-dependent photoluminescence spectrum at 1.4 K of sample 1. The luminescence is collected normal to the vicinal (100) surface of the sample, along the z direction as was defined in Fig. 1. The solid line shows the light emitted polarized parallel to the wires, along the x direction, and the dashed line the light emitted polarized perpendicular to the wires, along the y direction. The 15-Å QW and the $B(1)$ and $B(2)$ peaks seem to be isotropic whereas the A peak and the C band emit more light polarized along the direction of the wires.

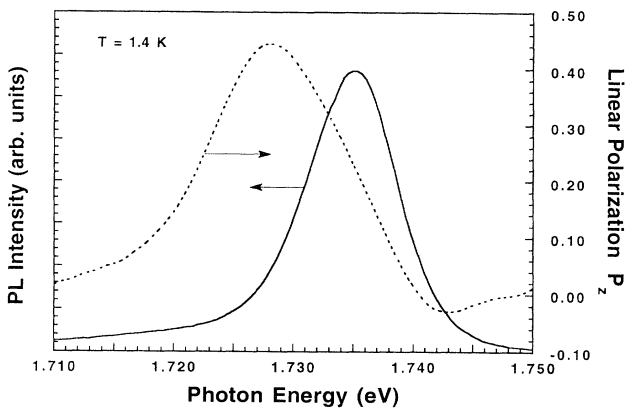

FIG. 7. Photoluminescence spectrum (solid line) and linear polarization P_z (dashed line), as defined in the text, of the 2° SSL peak in sample 2*b*. The SSL peak is mainly linearly polarized in the x direction (parallel to the wires) with a few percent linearly polarized in the y direction (perpendicular to the wires) at the high-energy side of the PL emission. The maximum of the linear polarization, 44%, is redshifted 7 meV from the PL peak where the polarization is 23%. The luminescence was emitted normal to the vicinal (100) surface and the pump intensity was about 10 W/cm^2.

wires whereas the $B(1)$ and $B(2)$ peaks and the reference 100-Å and 15-Å QW peaks seem to be isotropic. That the observed polarization is really due to the anisotropic properties of the sample has been proven by rotating the sample 90°, which rotated the PL signal by 90°. By using the definition of the linear polarization in Eq. (1), we find the linear polarization P_z of the A peak to be 30% and for the C band to be around 80–90 %.

To enhance the sensitivity of the polarization measurements and analyze the strength of the linear polarization in more detail we have used the PEM technique. In Fig. 7 the PL emission of the 2° SSL peak from sample 2*b* is shown together with the normalized value of the linear polarization P_z, as measured with the PEM. The pump intensity was close to 10 W/cm^2 in these measurements. It can be seen that most of the PL emission is linearly polarized in the x direction (parallel to the wires), with a few percent linearly polarized in the y direction (perpendicular to the wires) at the high-energy side of the PL emission. It can also be seen that the maximum of the linear polarization, 44%, is redshifted 7 meV from the PL peak where the polarization is 23%. The 0° SSL peak in sample 2*a* and the 60-Å and 80-Å QW peak did not show any linear polarization P_z.

The linear polarization of the PL emitted from the perpendicular directions has been measured by focusing the laser light onto the cleaved facets and analyzing the light emitted normal from the $(0\bar{1}1)$ surface (x direction) and normal from the (011) surface (y direction). The PL intensity was then measured at the peak of the emission, with the PEM switched off and on, while tuned to the first maximum of the second-order Bessel function and calculated by using Eq. (2). This has been determined for the A peak and the 100-Å QW peak in sample 1 and for the 2° SSL peak and the 60-Å QW peak in sample 2*b*, with the values of the linear polarization P_x,P_y, and P_z at *the peak of the PL emission* listed in Table II.

When the linear polarization spectra from the cleaved facets were measured, an interesting observation was that the energy position of the maximum polarization was red shifted for the SSL peaks (as seen for the P_z polarization in Fig. 7) whereas the energy position of the maximum polarization of the QW peaks coincided with the PL peak position.

Further, all the polarized PL spectra of sample 1 and 2 were independent of the polarization of the exciting laser light, a result that is expected from above-band-gap excitation (2.411 eV), whereby the carriers are frequently scattered (losing any polarization memory) before recombining in the SSL structure.

C. Linearly polarized photoluminescence excitation

The PLE (dotted line) and PL (dashed line) spectra at 1.4 K of the A peak in sample 1 are shown in Fig. 8. The spectrum is obtained by detecting at the low-energy side

TABLE II. Linear polarization of the PL [$P_x=(I_y-I_z)/(I_y+I_z)$, $P_y=(I_z-I_x)/(I_z+I_x)$, and $P_z=(I_x-I_y)/(I_x+I_y)$] emitted normal from the three perpendicular directions, as defined in the text, as measured at the peak of the PL emission. The measurements have been done on the SSL peaks as well as for the reference QW's.

Linear polarization	Sample 1		Sample 2*b*	
	A peak	100-Å QW	2° SSL	60-Å QW
P_x (%)	24	62	36	67
P_y (%)	−44	−70	−57	−76
P_z (%)	30	0	23	0

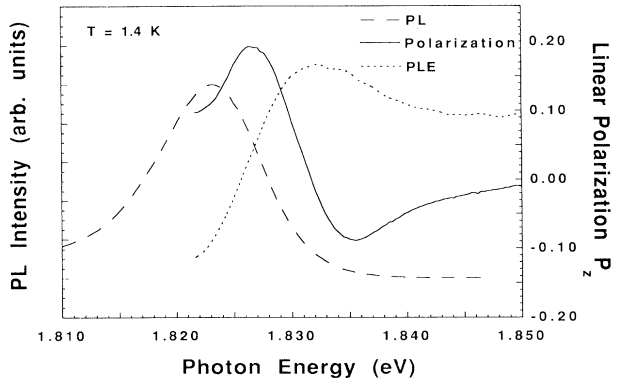

FIG. 8. Photoluminescence (dashed line) and photoluminescence excitation (dotted line) spectrum at 1.4 K of the A peak in sample 1. The solid line shows the linear polarization P_z of the PLE signal. At a few meV below the PLE peak, the absorption is stronger parallel to the wires (19%), and a few meV above the PLE peak the absorption is stronger perpendicular to the wires (−9%). At higher energies the absorption seems to be independent of the polarization of the exciting light. The laser excitation was normal to the vicinal surface and the pump intensity was about 10 W/cm^2.

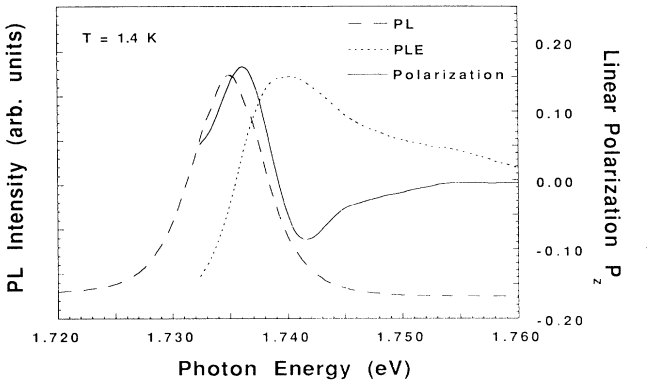

FIG. 9. Photoluminescence (dashed line) and photoluminescence excitation (dotted line) spectrum at 1.4 K of the 2° SSL peak in sample 2b. The solid line shows the linear polarization P_z of the PLE signal. At a few meV below the PLE peak, the absorption is stronger parallel to the wires (16%), and a few meV above the PLE peak, the absorption is stronger perpendicular to the wires (−7%). At higher energies the absorption seems to be independent of the polarization of the exciting light. The laser excitation was normal to the vicinal (100) surface and the pump intensity was about 10 W/cm^2.

(1.818 eV) of the SSL peak (A peak at 1.823 eV) and scanning the Ti:sapphire laser to higher energies. The laser excitation is ten times higher (10 W/cm^2) than was used to measure the spectrum in Fig. 3, saturating the B peaks. The laser excitation is normal to the vicinal (100) surface with the PEM used as shown in Fig. 2(b), while detecting the PLE signal at the chopper frequency, so that the horizontally polarized laser light from the Ti:sapphire is unpolarized before exciting the sample.[29] There is a broad Stokes shift of the ground-state transition of approximately 9 meV, with no indication of any higher subband structure. However, by using the PEM to directly measure the linear polarization of the PLE signal, a large anisotropy is observed around the absorption peak, as seen in Fig. 8 (solid line). At a few meV below the PLE peak, the absorption is stronger parallel to the wires (19%), and at a few meV above the PLE peak the absorption is stronger perpendicular to the wires (−9%). At higher energies the absorption seems to be independent of the polarization of the exciting light. The separation between the maximum and minimum polarization in Fig. 8 is found to be about 8.5 meV.

The PLE (dotted line) and PL spectra (dashed line) of the SSL peak in sample 2b are shown in Fig. 9. The laser excitation is normal to the vicinal (100) surface with the PEM used in the same way as was described above, with the detection at 1.731 eV. Again there is a broad Stokes shift of the ground-state transition (5.0 meV), with no indication of any higher subband structure. By using the PEM to measure the linear polarization of the PLE signal, a large anisotropy is observed around the absorption peak as shown in Fig. 9 (solid line). At a few meV below the absorption peak, the absorption is stronger parallel to the wires (16%), and a few meV above the absorption peak, the absorption is stronger perpendicular to the wires (−7%). At higher energies the absorption seems to be independent of the polarization of the exciting light. The separation between the maximum and minimum polarization in Fig. 9 is found to be about 4.6 meV. When the parallel and perpendicular excited PLE spectra are compared, the Stokes shifted peaks display a relative shift of 2.0 meV.

Neither the reference QW's nor the alloy-well peak in sample 2a showed any PLE anisotropy when excited normal to the vicinal (100) surface.

D. Intensity, lifetime, and uniformity of photoluminescence emission

The integrated intensity dependences of the A and $B(2)$ peaks and the C band of sample 1, as a functions of the laser power ($P_{\rm exc}$), are shown in a $\log_{10}(I_{\rm PL})$-$\log_{10}(P_{\rm exc})$ plot in Fig. 10. The pump power was varied from 0.1 to 14 W/cm^2 and the temperature was kept at 1.4 K. The solid lines are obtained by fitting the measured power dependence of the luminescence intensity by an $I_{\rm PL}\sim P_{\rm exc}^k$ law.[30] The A peak shows a super linear increase ($k=1.35$) whereas the $B(2)$ peak ($k=0.9$) and the C band ($k=0.7$) show a sublinear increase with increasing laser power.

The integrated PL intensity dependence of the 2° SSL peak in sample 2b as a function of the laser power ($P_{\rm exc}$) is shown in a $\log_{10}(I_{\rm PL})$-$\log_{10}(P_{\rm exc})$ plot in Fig. 11. The pump power was varied from 0.3 to 90 W/cm^2 and the temperature was kept at 1.4 K. The solid line is obtained by fitting the measured power dependence of the luminescence intensity by an $I_{\rm PL}\sim P_{\rm exc}^k$ law. This shows that the integrated SSL peak intensity varies linearly ($k=1.0$) with pump power over more than two orders of magnitude.

Decay-time measurements of the observed SSL peaks and the reference QW's have been performed at 1.6 K.

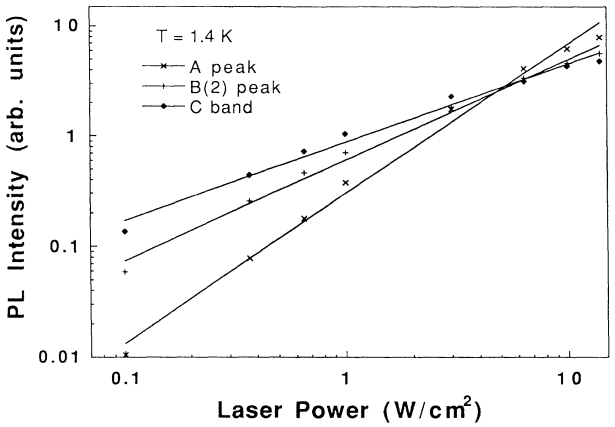

FIG. 10. The integrated photoluminescence intensity dependence of the A and $B(2)$ peak and the C band of sample 1, as a function of the laser power (P_{exc}). The pump power was varied from 0.1 to 14 W/cm^2 and the temperature was kept at 1.4 K. The solid lines are obtained by fitting the measured power dependence of the luminescence intensity by an $I_{\text{PL}} \sim P_{\text{exc}}^{k}$ law (Ref. 30). The A peak shows a superlinear increase ($k=1.35$) whereas the $B(2)$ peak ($k=0.9$) and the C band ($k=0.7$) show a sublinear increase with increasing laser power.

The PL emission intensity in sample 1 of the A, $B(1)$, $B(2)$ peaks and at three different energy positions of the C band, as a function of the time after the excitation pulse, are shown in Fig. 12. The sample was excited with 5-ps pulses at 2.104 eV using a Rhodamin 6 dye. The decay of the A peak, 6776-Å curve in Fig. 12(a), has an initial fast exponential decay, resulting in a lifetime of $\tau_{\text{pl}}=300\pm20$ ps, with a weak nonexponential tail. The exponential lifetime did not vary significantly by increasing the pump power by two orders of magnitude.

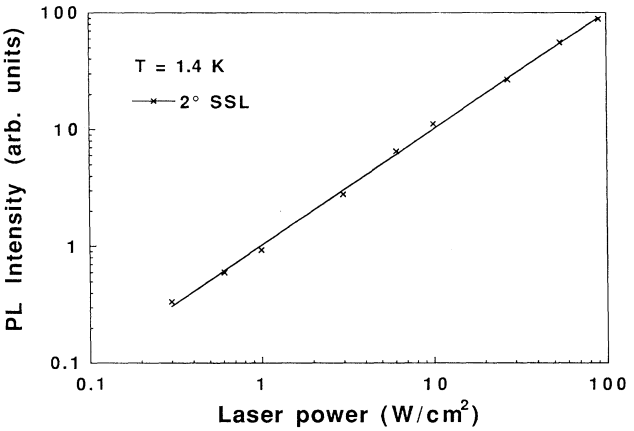

FIG. 11. The integrated PL intensity dependence of the 2° SSL peak in sample 2b as a function of the laser power (P_{exc}). The pump power was varied from 0.3 to 90 W/cm^2 and the temperature was kept at 1.4 K. The solid line is obtained by fitting the measured power dependence of the luminescence intensity by an $I_{\text{PL}} \sim P_{\text{exc}}^{k}$ law (Ref. 30). The integrated SSL peak intensity varies linearly ($k=1.0$) with pump power over more than two orders of magnitude.

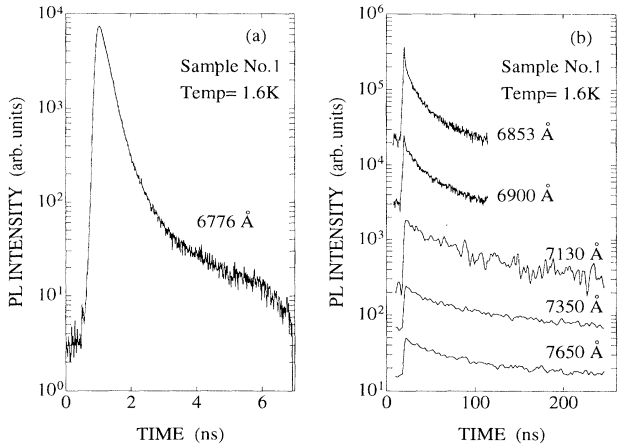

FIG. 12. (a) Measured decay time τ_{pl} in sample 1 of the A peak (6776 Å) as a function of the time after the excitation pulse. (b) Measured decay time τ_{pl} of the $B(1)$ and $B(2)$ peaks (6853 and 6900 Å, respectively) and at three different energy positions of the C band (7130, 7350, and 7650 Å). The sample was excited with 5-ps pulses at 2.104 eV using a Rhodamin 6 dye. The decay of the A peak has an initial fast exponential decay, resulting in a lifetime of $\tau_{\text{pl}}=300\pm20$ ps, with a weak nonexponential tail. The decay of the $B(1)$ and $B(2)$ peaks and the C band are all nonexponential and much longer.

The decay of the $B(1)$ and $B(2)$ peaks, 6853-Å and 6900-Å curves in Fig. 12(b), are both nonexponential and much longer than the A peak, resulting in a measured PL lifetime (measured as the time between maximum PL intensity and where the intensity has decreased by $1/e$) of 60 and 80 ns, respectively. The very fast initial decrease of the $B(1)$ peak is due to a spectral overlap of the decay from the A peak. The C band, measured at 7130, 7350, and 7650 Å in Fig. 12(b), also shows a nonexponential decay, which is increasing with decreasing energy, from 100 ns at 7130 Å to 400 ns at 7650 Å. The decay of the 100-Å QW showed an exponential decay time of about 400 ps, a value in agreement with previous studies of exciton recombination in QW's.[31]

The PL emission intensity of the 2° SSL peak in sample 2b and the alloy-well peak (0° SSL) in sample 2a as a function of the time after the excitation pulse is shown in Fig. 13. The sample was excited with 5-ps pulses at 1.823 eV using a Pyridine 2 dye. The decays of both peaks have a fast initial decay with a weak tail component with a much longer lifetime. By making exponential fits to the initial decays, result in lifetimes of $\tau_{\text{pl}}=390\pm20$ ps for the 2° SSL peak and $\tau_{\text{pl}}=260\pm20$ ps for the alloy-well peak. The 60-Å and 80-Å QW's had exponential decays with a measured PL decay time on both substrates of $\tau_{\text{pl}}=250\pm20$ ps, a value that is also in agreement with previous studies of exciton recombination in QW's.[31] The given exponential lifetimes are the best least-squares fits to the decay time measured between the points where the PL intensity has decreased to $\frac{1}{2}$ and $\frac{1}{20}$ (one order of magnitude) of the maximum PL intensity. It was also found that the lifetimes did not vary significantly by increasing the pump power by two orders of magnitude.

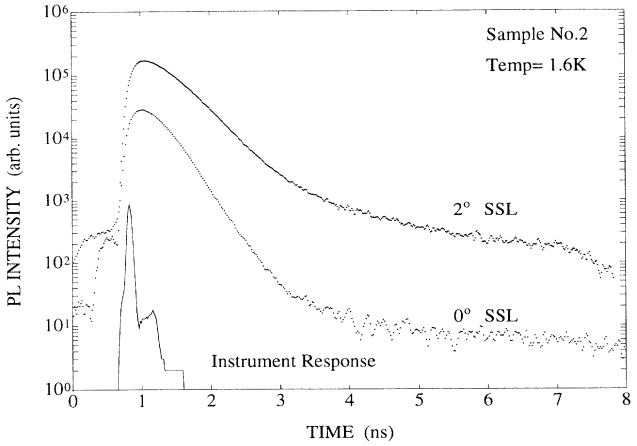

FIG. 13. Measured decay time τ_{pl} for the 2° SSL peak in sample 2*b* and the alloy-well peak (0° SSL) in sample 2*a*, as a function of the time after the excitation pulse. The sample was excited with 5-ps pulses at 1.823 eV using a Pyridine 2 dye. The decays of both peaks have a fast initial decay with a weak tail component with a much longer lifetime. By making exponential fits to the initial fast decays results in lifetimes of $\tau_{pl}=390\pm20$ ps for the 2° SSL peak and $\tau_{pl}=260\pm20$ ps for the alloy-well peak.

The peak position as a function of the spatial position in the *y* direction (*Ly*) for the *A* peak and the 15-Å QW peak in sample 1 are shown in Fig. 14. This sample was grown without any rotation, and it can be seen that there is a linear energy shift of the peak position for both peaks. The straight lines are least-squares fits to the data points giving a slope of 1.3 meV/mm for the *A* peak and 1.7 meV/mm for the 15-Å QW.

The PL peak energy position as well as the linear polarization of the 2° SSL emission as a function of the spatial position in the *y* direction (*Ly*) for sample 2*b* are shown in Fig. 15. This sample was grown under rotation,

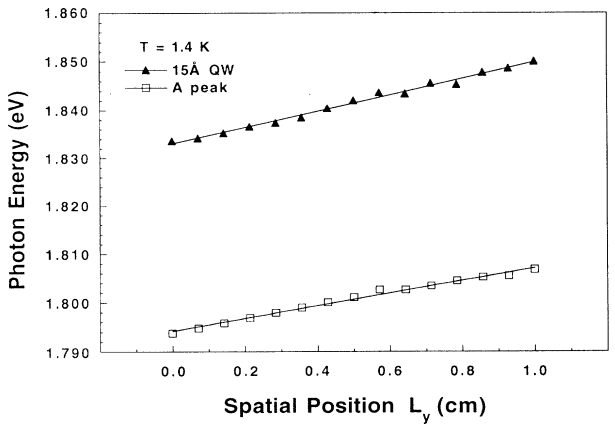

FIG. 14. The peak position vs spatial position in the *y* direction (L_y) for the *A* peak (open squares) and the 15-Å QW (filled triangles) in sample 1 (grown without rotation) at 1.4 K. The straight lines are least-squares fits to the data points giving a slope of 1.3 meV/mm for the *A* peak and 1.7 meV/mm for the 15-Å QW.

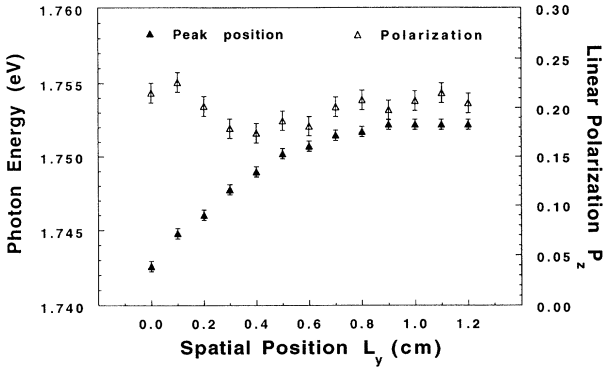

FIG. 15. The peak position (filled triangles) and linear polarization P_z (open triangles) vs spatial position in the *y* direction (L_y) for the 2° SSL peak in sample 2*b* (grown with rotation) at 1.4 K. The peak position is varying with about 1.5 meV/mm on one side of the sample and is almost uniform on the other side. The value of the linear polarization P_z seems to be independent of the PL peak position and varying with about ±3% around 20%, as measured at the same spatial positions.

and we find that the peak position is varying with about 1.5 meV/mm on one side of the sample and is almost uniform on the other. The value of the linear polarization P_z, as measured at the same spatial positions, seems to be independent of the peak position and varying with about ±3% around 20%.

IV. DISCUSSION

A. General photoluminescence properties

The recombination in the SSL structures is mainly radiative and the intrinsic PL from the SSL is excitonic. The excitonic PL lifetimes of the SSL *A* peak in sample 1 and the SSL peak in sample 2*b* are independent of the excitation intensity. Applying the principle of detailed balance in the steady state implies the lifetimes are independent of the concentration of free carriers generated by the exciting laser. The concentration-independent SSL lifetime is therefore that of *monomolecular* excitonic recombination.

When both radiative and nonradiative recombination are occurring and the available recombination channels are not saturated, the PL intensity I_{PL} for above bandgap excitation will exhibit a power-law dependence on the excitation power P_{exc}, $I_{PL}\sim P_{exc}^{k}$.[30,32] Again applying detailed balance, the power k will be between 1 and 2, where $k=1$ corresponds to when radiative recombination dominates and $k=2$ to when nonradiative recombination dominates. The SSL *A* peak of sample 1 has a superlinear intensity dependence, $k=1.35$, indicating a nonradiative contribution to the recombination. The linear PL intensity dependence, $k=1$, of the SSL peak in sample 2*b* for over two orders of magnitude indicates that recombination is dominated by radiative excitonic emission.

The *B* and *C* features in the PL spectra of sample 1 come from the SSL structure and are from defect-related

recombination. The CL line scan for peak A of Fig. 4 clearly associates this feature with the SSL layer. The $B(1)$ and $B(2)$ peaks and the C band are present only for excitation energies that are at or above the A peak energy, showing these spectral features are related to A and thus also come from the SSL structure. Luminescence from defects and impurities will saturate with excitation power as an appreciable fraction of the centers become occupied in steady state, giving $k<1$. Examples of this behavior include donor-acceptor pair (DAP) or free-to-bound (FB) emission.[32] The $B(2)$ peak, $k=0.9$, and C band, $k=0.7$, thus have the power dependences of defect-related luminescence. Long lifetimes are also an impurity signature and can be used to distinguish DAP and FB emission from bound-exciton emission, which will have a short lifetime close to that of free-exciton emission. The $B(1)$ and $B(2)$ peaks, with lifetimes of 60 and 80 ns, and the C band, with lifetimes of 100–400 ns, clearly behave as defect-related centers and could involve DAB or FB transitions to different impurity-trapped electrons or holes in the SSL structure. A DAP lifetime will be a decreasing function of energy as more distant pairs live longer due to the decreased overlap of the wave functions.[33] This is consistent with the C band lifetime dependence on the energy. More can be discerned about the B and C defects by considering their polarization. The B peaks did not show any linear polarization, which excludes free-hole-to-donor-electron transitions, but is consistent with free-electron-to-acceptor-hole and DAP transitions. The strong linear polarization of the C band of up to 90% along the wires can be due to a preferential defect orientation[34] and is probably not a SSL confinement effect. The defects which give the B and C spectral features may be due to an increase in unintentional impurities or to the AMBE growth of the SSL itself. Typical impurities in (Al,Ga)As MBE growth are carbon, as an acceptor, and oxygen, as a deep donor.[35] At the time that sample 1 was grown, the MBE machine had a very small intermittent leak, raising the base pressure to the mid-10^{-10}-Torr range, which could be an explanation for the defects. Furthermore, the concentrations of these impurities are expected to be higher in the SSL structure than for optimally grown MBE material because the effective SSL growth rate is more than an order of magnitude smaller. Foxon *et al.* have recently shown that AlAs/GaAs QW's grown by AMBE exhibit much more extrinsic recombination than if grown by SIMBE.[36] Defects related to the AMBE growth could include vacancies and antisite defects associated with turning off the As molecular beam. The PL spectrum of sample 2*b* shows, however, that the AMBE SSL growth may be accomplished without noticeable defect-related recombination at low temperature.

The measured linewidths of the 60-Å and 80-Å QW peaks (4–7 meV) are somewhat broader than normally observed, which is perhaps since they are not grown under conditions that are optimized for QW luminescence. We also notice that the 60-Å and 80-Å QW linewidths are somewhat broader on the 2° vicinal substrate compared to the flat substrate, probably induced by the pseudosmooth quality of the terraced (of 80 Å length) interfaces on the 2° substrate. However, this seems not to have affected the decay time of the excitons which showed similar lifetimes (250±20 ps) for the 60-Å and 80-Å QW on both substrates. The larger linewidth of the 2° SSL peak (7.5 meV) compared to the alloy-well peak (3.5 meV) is, however, a more dramatic effect than for the QW's, and is most likely due to the inhomogeneous fluctuations in the lateral SSL potential due to both geometrical and compositional variations.

B. Estimate of lateral intermixing and electronic structure from linear polarization of photoluminescence

The observation that the SSL emissions in the z direction are linearly polarized along the wires for Figs. 6 and 7 is in qualitative agreement with the selection rules for one-dimensional heavy-hole-to-electron transitions,[37] but can in principle also be caused by strain-induced effects or elongated island structures. We can rule out any strain-induced effects on the optical anisotropy, since the lattice mismatch between AlAs and GaAs is less than 0.1%.[8] Elongated island structures may also be ruled out because of the poor lateral separation of the material into GaAs wells and barriers. First this will reduce the lateral potential fluctuations that the carrier will experience, a reduction by more than an order of magnitude. Second, the higher Al alloy content of the layers pushes the valence-band confined states out from between the islands, reducing the degree to which the hole states experience the lateral fluctuations further. It is the hole states that cause the in-plane polarization dependence. Our calculations for the effect of elongated islands show explicitly that poor segregation minimizes the polarization effects of islands. Therefore we can with confidence claim that the linear polarization P_z observed for the SSL peaks is due to the lateral confinement of the excitons. This is also supported by the fact that the alloy-well peak and the QW transitions were all isotropic in this geometry.

The expected value of the polarization for the intended SSL structure (no lateral intermixing) depends on the exact geometry and actual potential of the crescent. This has been quantified by calculating the energies and wave functions for the SSL in the envelope approximation assuming decoupled conduction and valence-band states.[38] The optical polarization has then been calculated for the conduction-band to valence-band recombination. From TEM micrographs[27] we know that there is a substantial intermixing between the lateral barriers and wells, which we have introduced by calculating the optical polarization as a function of the amount of intermixing between the barrier and the well. This large intermixing will strongly modify the achieved electronic structure resulting in a weaker lateral confinement, which will weaken the polarization anisotropy and make it more two-dimensional-like. The intermixing has been considered by a rectangular composition profile (sharp interfaces) where the Al is uniformly removed and uniformly redistributed into the well. The linear polarization (P_x, P_y, and P_z) has then been calculated in all three perpendicular directions for the electron–heavy-hole transition

(solid lines) and electron–light-hole transition (dashed lines) as a function of the difference in the Al composition in the SSL barrier and well, $\Delta x = x_{\text{barrier}} - x_{\text{well}}$, as plotted in Fig. 16 for sample 1 and 2*b*. It should be noted that we can expect considerable polarization even for relatively large intermixing. By using the experimentally determined values of the linear polarization (Table II) of the PL indicated by the plus marks in Fig. 16, the actual amount of intermixing between the lateral barriers and wells in the SSL structure has been estimated. The inferred amount of intermixing in the three perpendicular directions are in rough agreement with each other. For sample 1 we get an average composition difference $\Delta x \approx 0.054$ ($x_{\text{barrier}} = 0.245$, $x_{\text{well}} = 0.191$) compared to the intended $\Delta x = 0.50$. For sample 2*b* we get an average composition difference $\Delta x \approx 0.081$ ($x_{\text{barrier}} = 0.207$, $x_{\text{well}} = 0.126$) compared to the intended $\Delta x = 0.333$.

The lateral composition modulations obtained from the calculations may be expressed as lateral energy barrier heights. Assuming that an alloy difference of $\Delta x = 0.3$ corresponds linearly to a 240-meV conduction-band offset, we get a lateral potential-energy barrier height in the conduction band of approximately 40 and 60 meV for samples 1 and 2*b*, respectively. According to our calculations this indicates that the hole states are confined to 1D

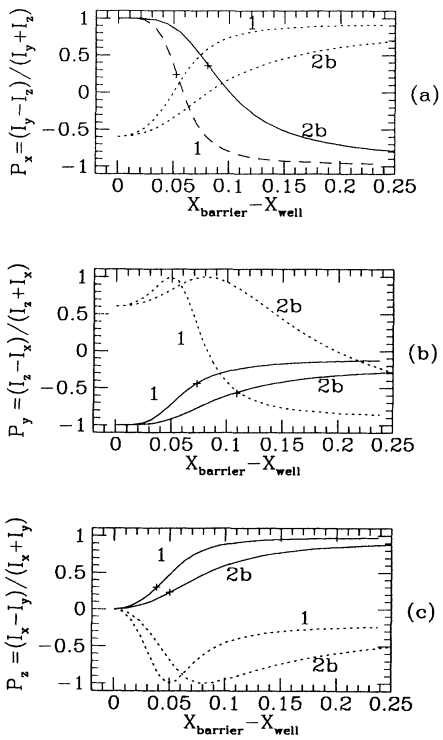

FIG. 16. Calculated linear polarization (a) P_x, (b) P_y, and (c) P_z for the electron heavy-hole transition (solid lines) and electron light-hole transition (dashed lines) as a function of the difference in the Al composition in the SSL barrier and well $x_{\text{barrier}} - x_{\text{well}}$. The experimentally determined values of the linear polarization (Table II) of the PL in samples 1 and 2*b* are indicated by the plus marks. The inferred segregations in the three perpendicular directions are in rough agreement with each other.

while the electron states are coupled through the lateral barriers because of the lighter effective mass and are confined to 2D. It should be noted that we have used the linear polarization values at the SSL peak position, which is not at the maximum of the polarization, as was seen in Fig. 7. The linear polarization peak has been found to be redshifted from the PL peak, achieving a linear polarization of almost a factor 2 larger at the low-energy tail of the SSL emission, in all the samples we have studied so far. This indicates that there is a distribution of quantum wires with different quality within the SSL peak. More wirelike states (due to, e.g., a larger local segregation) with a larger lateral confinement would lead to a larger polarization and a lower ground-state transition energy.

The values of the linear polarization P_x and P_y of the 60-Å QW are expected to be polarized 100% along the QW plane, but experimentally values around 70% were observed (Table II). This breakdown of the optical selection rules for excitons in QW's has been reported previously and explained to be due to valence-band mixing effects of the exciton wave function,[39] which has not been included in our calculations so far. Valence-band mixing will of course also affect the optical selection rules in the samples investigated here. We also have to keep in mind other effects that might lower the linear polarization, such as structural irregularities of the wires. The Stokes shift between the PL and the PLE peaks indicates that the excitons in the SSL structures are not free, but rather localized in potential fluctuations similar to what is typically observed for excitons in QW's.[40] This localization of the free exciton will reduce the linear polarization. Therefore by using the measured linear polarization as described above this will *overestimate* the amount of the intermixing.

C. Lateral confinement effects on linear polarized photoluminescence excitation, recombination lifetime, and energy shift

As was shown in Figs. 8 and 9 the PLE spectra did not show any structure that could be directly assigned to any higher one-dimensional subbands nor any heavy-hole–light-hole splitting. This is not surprising because the linewidths of the SSL peaks [11 meV for sample 1 (Fig. 8) and 7 meV for sample 2*b* (Fig. 9)] are greater than the expected subband splittings. The first-to-second electron subband spacing is close to 5 meV for the lateral conduction-band potential calculated for the intermixed SSL's above. However, from the polarized PLE experiments and by referring to the calculated electron–light-hole transition as a function of the intermixing (dashed lines in Fig. 16), we have other evidence for the lateral confinement in the SSL structure. From Fig. 16 it was observed that for light traveling in the *z* direction the heavy-hole state is resonantly excited with light parallel to the wire and the light-hole state with light perpendicular to the wire. This is in qualitative agreement with the linear polarization P_z of the PLE as was observed in Figs. 8 and 9, where the positive maximum would correspond to the electron–heavy-hole state and the negative minimum to the electron–light-hole state. We therefore

take the peak shift between the maximum and minimum polarization as an indication of the heavy-hole–light-hole splitting. However, because of the rather broad linewidth of the SSL peaks and the nonresonant signal contribution to the resonant signal, this separation is likely to be overestimated.

When analyzing the PL decay times it should be noted that the measured lifetime in the experiments is the total decay time $\tau_{\rm pl}$, which is related to the radiative τ_r and nonradiative decay time $\tau_{\rm nr}$ by

$$1/\tau_{\rm pl}=1/\tau_r+1/\tau_{\rm nr} . \quad (3)$$

Comparing the measured lifetime for the 2° SSL peak (390 ps) and the alloy-well peak in sample 2 (260 ps), we find that the measured lifetime at 1.6 K is longer in the serpentine sample than in the alloy-well sample. The lifetime at low temperatures was systematically found to be longer from the 2° SSL peak than from any of the QW's or the 0° SSL peak in sample 2. This seems to indicate that the exciton recombination rate is reduced in the serpentine structure, which is consistent with calculations by Citrin of exciton recombination in quantum wires.[41] In our case this longer lifetime can be explained by the significant mismatch between the electron and hole wave function in the SSL structure compared to the alloy quantum well.[42] The interpretation gets, however, further complicated by the fact the SSL excitons are localized in potential fluctuations, which also tends to increase the recombination lifetime,[41] and it is not possible at this point to say which effect that dominates. This preliminary lifetime study is now being extended with a more detailed study (including the temperature dependence) on specially designed SSL samples, which will be published elsewhere.

The SSL PL peak energy will be lower in energy than a corresponding alloy structure, where the redshift depends on the SSL geometry and the amount of composition modulation. To verify if the SSL peak is redshifted compared to a similarly grown alloy well, the 60-Å and 80-Å QW's in sample 2 were used as markers to ensure that the growth rate has been about the same. From Fig. 5 it can be seen that the 2° SSL peak is redshifted with about 12 meV compared to the alloy-well peak grown on the flat substrate. These spectra were intentionally measured on spatial positions that made the QW's to line up at the same energy position. The QW peak position can be determined to an accuracy of 5% of the FWHM or to about ±0.35 meV for the 60-Å QW. Such an energy shift could be caused by either a thickness variation of the GaAs well width or a composition change in the $Al_{0.3}Ga_{0.7}As$ barrier (or a combination of both). A 0.35-meV QW shift can occur if the Ga and Al growth rates are off causing a composition change in the barrier of $\Delta x=\pm 0.005$. This means that the average alloy composition in the 2° SSL sample and the alloy-well sample can be off by about $\Delta x=\pm 0.005$ at the points where the 60-Å QW peaks seem to line up. By using the calculations of the band gap vs composition for $Al_xGa_{1-x}As$ alloys by Aspnes *et al.*,[43] the band gap (the Γ band) is found to shift with about 7 meV for a change in the Al composition by $\Delta x=0.005$. Therefore even if we attribute 7 meV of the observed 12-meV redshift in Fig. 5 to be due to a growth rate difference, at least 5 meV must be due to the lateral confinement in the 2° SSL sample. This is true under the assumption that the peak position of the SSL is largely determined by the average Al composition in the SSL layers. For a 5-meV energy shift we calculate $\Delta x=0.10$ in the SSL ($x_{\rm barrier}=0.218$, $x_{\rm well}=0.115$), which corresponds to a potential-energy difference between the barrier and the well of approximately 82 meV in the conduction band. This is a somewhat larger potential difference than was estimated from the PL polarization, which was argued to underestimate the potential difference.

D. SSL uniformity: Insensitivity to growth-rate variations

The four arrays of crescents in sample 1 were intended to be formed while the coverage changed from 1.1 to 0.9 monolayers over the 102-nm span of the arcs. From the TEM micrograph (Fig. 1 in Ref. 25) it was estimated that the actual range of coverage was from 1.15 to 0.95 monolayers over the span of arcs. This shows that there is a systematic error of 5% in the nominal coverage, which still gave the intended SSL cross section, only shifting the crescents upwards and downwards. The intended average Al composition in the SSL structure in sample 1 is 21.4%, which corresponds to a band gap of about 1.829 eV.[43] Our data show that the *A* peak can be observed at energies from about 1.794 to 1.823 eV depending on the spatial position (Figs. 3 and 14). With the amount of intermixing that was estimated for the SSL structure in sample 1 (Sec. IV B) the PL peak is expected to be redshifted by only 2–3 meV from the band gap of an alloy with the same average Al composition. Including some redshift due to the exciton binding energy (5 meV), we estimate the average Al composition to be varying from about 19% (at 1.794 eV) to close to the intended 21.4% (at 1.823 eV) across the wafer. The TEM micrograph which showed a 5% nominal increase in the monolayer coverage indicates a higher Al and/or Ga growth rate than the intended. To be consistent with the PL results it seems like the Ga growth rate has been slightly larger than intended across most of the wafer.

The intended Al composition in the alloy-well structure in sample 2*a* was 16.7%, which corresponds to a band gap of about 1.776 eV.[43] Adding the energy due to the vertical confinement (16 meV for a QW with well width 510 Å) and subtracting for the exciton binding energy (4 meV), the expected PL peak position should be close to 1.788 eV. The observed peak position of the alloy-well was at 1.747 eV in Fig. 5, which corresponds to a decrease in the Al composition of $\Delta x=0.03$, which indicates that there is a decrease in the Al growth rate and/or an increase in the Ga growth rate. The growth rate in the SSL structure in sample 2*b* is probably off by a similar amount, since the QW peaks were used as markers in Fig. 5 to ensure that the alloy compositions were fairly similar.

From Fig. 14 it can be seen that the SSL peak energy shift in sample 1 (*A* peak) is about the same as the nar-

row 15-Å QW. Sample 1 was grown without rotation and is expected to have spatial variations of the growth rate on the substrate, due to the spatial dependence on the distance and angle to the Al and Ga source. The variation of the Al composition has been estimated from the slope in Fig. 14 and by using the calculations of the band gap vs. composition by Aspnes *et al.*[43] By assuming that the peak position of the SSL is largely determined by the average Al composition in the SSL layer, the energy shift (1.3 meV/mm) of the A peak corresponds to a variation of the Al composition in the SSL region of about $\Delta x = 0.01$ across 1 cm of the sample. This spatial variation of the Al composition can be overcome somewhat if the sample is grown under rotation, as was done for sample 2, shown in Fig. 15. The rotation of the sample was synchronized with the molecular-beam shutters as explained in Sec. II A. As can be seen in Fig. 15 this may result in regions with almost no variation in the peak position of the SSL (between position 0.6 and 1.2 cm as observed in Fig. 15). On the other hand, some regions see variations similar to the shifts observed in sample 1 (1.5 meV/mm between position 0.0 and 0.6 cm in Fig. 15). The 10-meV energy shift across 1.2 cm of sample 2b corresponds to a variation of the Al composition in the SSL region of $\Delta x = 0.008$. More important, however, is the uniformity of the linear polarization observed over the same region in the sample. The linear polarization P_z is found to be close to $20 \pm 3\%$, and seemingly independent of the SSL peak position. This means that quantum-wire-like states are formed over large regions of the sample, independently of the variations of the growth rate that was observed on one side of the sample. This shows the intended advantage of the SSL structure compared with the tilted superlattice, where the linear polarization is weaker and not very uniform,[44] so that there are even locations with no linear polarization P_z (where the TSL's are strongly tilted). This is due to the sensitivity of the tilt angle on variations of the growth rate for the TSL, which is inherently accommodated by the SSL geometry.

V. SUMMARY AND CONCLUSIONS

The growth and optical properties of serpentine superlattice structures that have a built in quantum-wire array have been described. The structures have been characterized by low-temperature cathodoluminescence, photoluminescence, and photoluminescence excitation measurements. In PL we observe a redshifted peak that we can attribute to excitonic recombination in the built-in quantum-wire array. The linear polarization dependence of the SSL emission has been measured with a photoelastic modulation technique, which shows a pronounced polarization anisotropy in both PL and PLE. The serpentine PL emission shows a linear polarization along the wires of up to about 30% due to the lateral confinement. The measured polarization anisotropy has been compared with the calculated polarization dependence as a function of segregation between the lateral barriers and wells. It is found that there is a substantial intermixing between the lateral barriers and wells, with at least 30% of the Al intended for the barrier ending up in the well. This results in hole states confined to 1D, while the electron states are 2D due to coupling through the lateral barriers. From linear polarized PLE we have been able to reveal the laterally induced heavy-hole–light-hole splitting. PL decay time measurements of the SSL structure (390 ps) show a longer (radiative) decay time than for a reference alloy-well structure (260 ps) at 1.6 K, indicating a reduced recombination rate in the serpentine structure. The linear polarization of the photoluminescence is found to be rather constant over large areas of the wafer even though the growth rate is varying with a few percent. This indicates that uniform quantum-wire-like states are formed and demonstrates the intended advantage of the serpentine superlattice which avoids the tilt sensitivity of the tilted superlattice. The principal limitation of the SSL structures grown to date is the amount of intermixing between Al and Ga on the terraces. This problem might be improved by growing on other vicinal surfaces than (100), such as the (110) (Ref. 45) and (111)B planes. Also there are other III-V compound semiconductor systems to explored, such as the (Al,Ga)Sb system that has recently indicated an improved segregation over the (Al,Ga)As system.[46,47]

In this paper we have also described an all optical technique that allows the lateral confinement (and amount of intermixing) of these structures to be determined and should be very useful in any future studies aimed to improve the growth of SSL and TSL structures.

ACKNOWLEDGMENTS

We want to thank M. Wassermeier for discussions on the use of a photoelastic modulator in the polarization measurements, and B. Monemar for a critical reading of the manuscript. One of the authors (H.W.) acknowledges support from the Swedish Research Council for Engineering Sciences (TFR) and the NSF-Science and Technology Center for Quantized Electronic Structures (QUEST), Grant No. DMR 91-20007. Part of the work of H.W. was performed while at QUEST, University of California, Santa Barbara, CA 93106.

[1]H. Sakaki, Jpn. J. Appl. Phys. **19**, 94 (1980).

[2]M. Kohl, D. Heitman, P. Grambow, and K. Ploog, Phys. Rev. Lett. **63**, 2124 (1989).

[3]M. Notomi, M. Naganuma, T. Nishida, T. Tamamura, H. Iwamura, S. Nojima, and M. Okamoto, Appl. Phys. Lett. **58**, 720 (1991).

[4]H. Hirayama, Y. Suzuki, S. Tarucha, and H. Okamoto, Jpn. J. Appl. Phys. **24**, L516 (1985).

[5]J. M. Gaines, P. M. Petroff, H. Kroemer, R. J. Simes, R. S. Geels, and J. H. English, J. Vac. Sci. Technol. B **6**, 1378

(1988).
[6]E. Kapon, D. M. Hwang, and R. Bhat, Phys. Rev. Lett. **63**, 430 (1989).
[7]R. Cingolani, H. Lage, L. Tapfer, H. Kalt, D. Heitmann, and K. Ploog, Phys. Rev. Lett. **67**, 891 (1991).
[8]K. Kash, B. P. Van der Gaag, D. D. Mahoney, A. S. Gozdz, L. T. Florez, J. P. Harbison, and M. D. Sturge, Phys. Rev. Lett. **67**, 1326 (1991).
[9]K. Kash, J. Lumin. **46**, 69 (1990), and references therein.
[10]G. Mayer, H. Leier, B. E. Maile, A. Forchel, H. Schweizer, G. Weimann, and W. Schlapp, *Proceedings of the 20th International Conference on the Physics of Semiconductors, Thessaloniki, Greece, 1990,* edited by E. M. Anastassakis and J. D. Joannopoulus (World Scientific, Singapore, 1991), pp. 2415–2418.
[11]D. S. Citrin and Y.-C. Chang, Phys. Rev. B **43**, 11 703 (1991); J. Appl. Phys. **69**, 2685 (1991).
[12]P. C. Sercel and K. J. Vahala, Phys. Rev. B **44**, 5681 (1991).
[13]U. Bockelmann and G. Bastard, Europhys. Lett. **15**, 215 (1991).
[14]D. Gershoni, J. S. Weiner, S. N. G. Chu, G. A. Baraff, J. M. Vandenberg, L. N. Pfeiffer, K. West, R. A. Logan, and T. Tanbun-Ek, Phys. Rev. Lett. **65**, 1631 (1990).
[15]R. Nötzel, N. N. Ledentsov, L. Däweritz, M. Hohenstein, and K. Ploog, Phys. Rev. Lett. **67**, 3812 (1991).
[16]E. Kapon, K. Kash, E. M. Clausen, Jr., D. M. Hwang, and E. Colas, Appl. Phys. Lett. **60**, 477 (1992).
[17]K. Kash, D. D. Mahoney, and H. M. Cox, Phys. Rev. Lett. **66**, 1374 (1991).
[18]K. Kash, J. M. Worlock, A. S. Gozdz, B. P. Van der Gaag, J. P. Harbison, P. S. D. Lin, and L. T. Florez, Surf. Sci. **229**, 245 (1990).
[19]T. Fukui and H. Saito, J. Vac. Sci. Technol. B **6**, 1373 (1988).
[20]M. Tsuchiya, J. M. Gaines, R. H. Yan, R. J. Simes, P. O. Holtz, L. A. Coldren, and P. M. Petroff, Phys. Rev. Lett. **62**, 466 (1989).
[21]H. Weman, M. S. Miller, and J. L. Merz, Phys. Rev. Lett. **68**, 3656 (1992).
[22]M. Tanaka and H. Sakaki, Appl. Phys. Lett. **54**, 1326 (1989).
[23]G. E. W. Bauer and H. Sakaki, Phys. Rev. B **44**, 5562 (1991).
[24]M. S. Miller, C. Pryor, H. Weman, L. A. Samoska, H. Kroemer, P. M. Petroff, and J. L. Merz, J. Cryst. Growth **111**, 323 (1991).
[25]M. S. Miller, H. Weman, C. E. Pryor, M. Krishnamurthy, P. M. Petroff, H. Kroemer, and J. L. Merz, Phys. Rev. Lett. **68**, 3464 (1992).
[26]H. Weman, E. D. Jones, C. R. McIntyre, M. S. Miller, P. M. Petroff, and J. L. Merz, Superlatt. Microstruct. **13**, 5 (1993).
[27]M. Krishnamurthy, M. S. Miller, and P. M. Petroff, Appl. Phys. Lett. **61**, 2990 (1992).
[28]Y. Horikoshi, M. Kawashima, and H. Yamaguchi, Jpn. J. Appl. Phys. **27**, 169 (1988).
[29]M. Wassermeier, H. Weman, M. S. Miller, P. M. Petroff, and J. L. Merz, J. Appl. Phys. **71**, 2397 (1992).
[30]T. Taguchi, J. Shirafuji, and Y. Inuishi, Phys. Status Solidi B **68**, 727 (1975).
[31]J. Feldmann, G. Peter, E. O. Göbel, P. Dawson, K. Moore, C. Foxon, and R. J. Elliot, Phys. Rev. Lett. **59**, 2337 (1987).
[32]T. Schmidt, K. Lischka, and W. Zulehner, Phys. Rev. B **45**, 8989 (1992).
[33]F. Williams, Phys. Status Solidi **25**, 493 (1968).
[34]M. S. Skolnick, T. D. Harris, C. W. Tu, T. M. Brennan, and M. D. Sturge, Appl. Phys. Lett. **46**, 427 (1985).
[35]H. Künzel and K. Ploog, Appl. Phys. Lett. **37**, 416 (1980).
[36]C. T. Foxon, D. Hilton, P. Dawson, K. J. Moore, P. Fewster, N. L. Andrew, and J. W. Orton, Semicond. Sci. Technol. **5**, 721 (1990).
[37]C. R. McIntyre and L. J. Sham, Phys. Rev. B **45**, 9443 (1992).
[38]C. Pryor, Phys. Rev. B **44**, 12 912 (1991).
[39]J. S. Weiner, D. S. Chemla, D. A. B. Miller, H. A. Haus, A. C. Gossard, W. Wiegman, and C. A. Burrus, Appl. Phys. Lett. **47**, 664 (1985).
[40]G. Bastard, C. Delalande, M. H. Meynadier, P. M. Frijlink, and M. Voos, Phys. Rev. B **29**, 7042 (1984).
[41]D. S. Citrin, Phys. Rev. Lett. **69**, 3393 (1992).
[42]J. C. Yi, H. Weman, M. S. Miller, N. Dagli, P. M. Petroff, and J. L. Merz (unpublished).
[43]D. E. Aspnes, S. M. Kelso, R. A. Logan, and R. Bhat, J. Appl. Phys. **60**, 754 (1986).
[44]H. Weman, M. S. Miller, P. M. Petroff, H. Kroemer, and J. L. Merz, Bull. Am. Phys. Soc. **36**, 824 (1991).
[45]M. Krishnamurthy, M. Wassermeier, H. Weman, J. L. Merz, and P. M. Petroff, in *Interface Dynamics and Growth,* edited by K. S. Liang, M. P. Anderson, R. F. Bruinsma, and G. Scoles, MRS Symposia Proceedings No. 237 (Materials Research Society, Pittsburgh, 1992), p. 473.
[46]S. A. Chalmers, H. Kroemer, and A. C. Gossard, Appl. Phys. Lett. **57**, 1751 (1990).
[47]S. A. Chalmers, H. Weman, J. C. Yi, H. Kroemer, J. L. Merz, and N. Dagli, Appl. Phys. Lett. **60**, 1676 (1992).